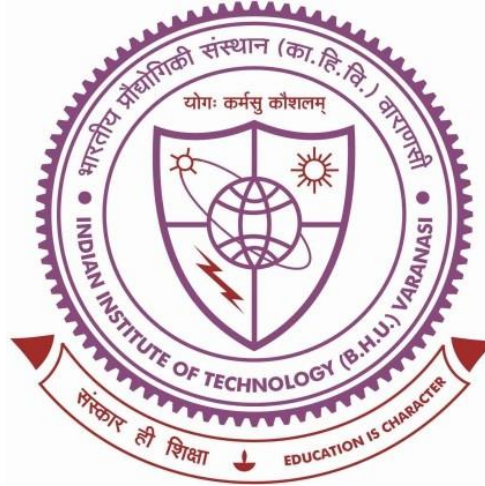


FABRICATION AND TRIBOLOGICAL CHARACTERIZATION OF Ni ALLOY-BASED SELF-LUBRICATING HYBRID COMPOSITES



**Thesis submitted in partial fulfillment for the
Award of Degree**

Doctor of Philosophy

By

Smita Gupta

**DEPARTMENT OF MECHANICAL ENGINEERING
INDIAN INSTITUTE OF TECHNOLOGY
(BANARAS HINDU UNIVERSITY)
VARANASI - 221005
INDIA**

Roll No. 19131009

2024

CERTIFICATE

This is to certify that the work contained in the thesis title “ *FABRICATION AND TRIBOLOGICAL CHARACTERIZATION OF Ni ALLOY-BASED SELF-LUBRICATING HYBRID COMPOSITES* ” by “ *SMITA GUPTA* ” has been carryout under our supervision that this work has not been submitted elsewhere for a degree.

It is further certified that the student has fulfilled all the requirements of Comprehensive Examination, Candidacy and SOTA for the award of Ph.D. Degree.

Supervisor
(Prof. Rajnesh Tyagi)
IIT(BHU), Varanasi

Co-Supervisor
(Prof. P. K. Jain)
IIT, Roorkee

Co-Supervisor
(Dr. O. P. Khatri)
CSIR-IIP, Dehradun

DECLARATION BY THE CANDIDATE

I, “**SMITA GUPTA**”, certify that the work embodied in this thesis is my own bonafede work and carried out by me under the supervision of “**Prof. Rajnesh Tyagi, Prof. P. K. Jain, and Dr. O.P. Khatri**” from “**July 2019**” to “**December 2024**”, at the “**Department of Mechanical Engineering, Indian Institute of Technology (BHU), Varanasi, India**” and “**CSIR – Indian Institute of Petroleum, Dehradun, India**”. The matter embodied in this thesis has not been submitted for the award of any other degree/diploma.

I declare that I have faithfully acknowledged and given credits to the research workers wherever their works have been cited in my work in this thesis. I further declare that I have not wilfully copied any other’s work, paragraphs, text, data, results, etc., reported in journals, books, magazines, reports dissertations, theses, etc., or available at websites and have not included them in this thesis and have not cited as my own work.

Date: 26-12-24

Place: Varanasi


(SMITA GUPTA)

CERTIFICATE BY THE SUPERVISORS

It is certified that the above statement made by the student is correct to the best of our knowledge.



Supervisor
(Prof. Rajnesh Tyagi)
IIT(BHU), Varanasi



Co-Supervisor
(Prof. P. K. Jain)
IIT, Roorkee



Co-Supervisor
(Dr. O. P. Khatri)
CSIR-IIP, Dehradun


Signature of Head of Department
विभागाध्यक्ष/HEAD

यान्त्रिक अभियान्त्रिकी विभाग/Deptt. of Mechanical Engg.
भारतीय प्रौद्योगिकी संस्थान/Indian Institute of Technology
(का०हि०वि०/B.H.U.)
वाराणसी-221005/Varanasi-221005

COPYRIGHT TRANSFER CERTIFICATE

Title of the Thesis: Fabrication and Tribological Characterization of Ni Alloy-Based Self-Lubricating Hybrid Composites

Name of the Student: SMITA GUPTA

Copyright Transfer

The undersigned hereby assigns to the Indian Institute of Technology (Banaras Hindu University), Varanasi all rights under copyright that may exist in and for the above thesis submitted for the award of the **Doctor of Philosophy**.

Date: 26-12-24

Place: Varanasi



(SMITA GUPTA)

Note: However, the author may reproduce or authorize others to reproduce material extracted verbatim from the thesis or derivative of the thesis for author's personal use provided that the source and the Institute's copyright notice are indicated.

ACKNOWLEDGEMENT

The author is pleased to express her sincere thanks and gratitude beyond words to her supervisor Prof. Rajnesh Tyagi and co-supervisors, Prof. Pramod Kumar Jain, and Dr. Om Prakash Khatri for their consistent help, encouragement and valuable discussions during the entire period of her research work. The author would not have been able to complete the thesis without their utmost involvement and invaluable efforts. They motivated the author to pursue research problems and the need for persistent effort to accomplish the goal. The author is truly indebted to them.

Besides supervisors, the author would like to thank her RPEC members, Prof. Sunil Mohan (Metallurgical Engineering Department) and Prof. Rakesh Kumar Gautam for their insightful comments and encouragement. The author acknowledges her immense sense of gratitude to the current and former Heads of the Department of Mechanical Engineering for providing all the research facilities to accomplish her research in the Department successfully. The author has an immense sense of gratitude to all the faculty members of the Department of Mechanical Engineering, IIT (BHU), Varanasi for their cooperation and inspiration.

The author is highly obliged and wishes to express her sincere thanks to Dr. Om Prakash Khatri (Indian Institute of Petroleum, CSIR) for allowing him to work in the Tribology Laboratory, IIP Dehradun as a non-degree student. The author also wishes to record her sincere thanks to Ms. Anchal Pandey for lending the continuous support during her work in IIP. The author is also thankful to all her friends, lab and office staff of the Indian IIP.

The author is thankful to the unknown reviewers who have rejected my papers several times in journals. The comments that they provided helped polish our articles and

put them in better shape. Nevertheless, the bigger and nobler cause of thanking them is that the rejections have equipped me with a high level of patience and helped me to implement my spiritual thoughts in practice. My acknowledgement will never be complete without the special mention to my lab seniors and colleagues for their great help during five years of the Ph.D. journey- Dr. Pooja, Dr. Nitish, Dr. Chitrance, Dr. Jyoti, Mr. Abhay and seniors I convey my gratitude to all my teachers throughout my academic career for preparing me to walk through this long journey. The author is also thankful to all the lab, workshop, CIFIC, and office staff of the department, especially Mr. Vijay Pratap Srivastava (CAM lab) and Aman, Sachin and Sudhakar (CIFIC lab). I want to thank the administrative personnel at IIT BHU for helping me with their expertise during several requirements that had to be met over the entire course of the Ph.D. at IIT BHU.

Last but not least, words fail me to express my appreciation when it is time to share my gratitude to those very special people who always stood like a pillar of strength, Last but not least, words fail me to express my appreciation when it is time to share my gratitude to those very special people, who always stood like a pillar of strength, my loveable daughter Ms. Mishika Sharma, husband Mr. Yagik Sharma, brother Mr. Arpit Gupta, in-laws Mr. Ravinder Sharma and Smt. Sunita Sharma, and parents Mr. Umesh Kumar Gupta and Smt. Pushpa Gupta.

At last, thanks to the almighty God who has given the author spiritual support and courage to carry out this work.



(SMITA GUPTA)

Table of Contents

Contents	Page No.
List of Figures	<i>xiii</i>
List of Tables	<i>xxi</i>
List of Abbreviations/Symbols	<i>xxii</i>
Preface	<i>xxiv</i>
Chapter 1: INTRODUCTION	1
Chapter 2: REVIEW OF LITERATURE	7
2.1 COMPOSITE AND ITS TYPES	7
2.2 PROCESSING TECHNIQUES FOR COMPOSITES	9
2.2.1 Liquid State Processing	9
2.2.2 Solid State Processing	10
2.2.2.1 Powder metallurgy (P/M)	10
2.2.2.2 Diffusion bonding	14
2.2.2.3 Deposition processing	14
2.2.2.4 In-situ processing	15
2.2.3 Spark Plasma Sintering (SPS)	16
2.3 TRIBOLOGY	17
2.4 WEAR AND ITS TYPES	18
2.5 FACTORS GOVERNING WEAR	19
2.6 LUBRICATION	22
2.7 NEED FOR SOLID LUBRICATION AT ELEVATED TEMPERATURE	28
2.8 SELF-LUBRICATING MATERIALS FOR HIGH TEMPERATURE APPLICATIONS	29

2.9	<i>FORMULATION OF THE PROBLEM</i>	38
Chapter 3: <i>EXPERIMENTAL PROCEDURE</i>		42
3.1	<i>RAW MATERIALS</i>	42
3.2	<i>SYNTHESIS OF REINFORCEMENTS</i>	43
3.2.1	<i>Reduced Graphene Oxide (rGO) and Ni-doped rGO (rGO-Ni)</i>	43
3.2.2	<i>Ni-doped Hexagonal Boron Nitride (h-BN-O-Ni)</i>	45
3.2.3	<i>Characterisation of rGO, rGO-Ni, and h-BN-Ni</i>	47
3.2.3.1	<i>Fourier-transform infrared spectrometer (FTIR) analysis</i>	47
3.2.3.2	<i>X-ray diffraction (XRD) analysis</i>	47
3.2.3.3	<i>Raman spectroscopy</i>	48
3.2.3.4	<i>Transmission electron microscopy (TEM)</i>	48
3.2.3.5	<i>X-ray photoelectron spectroscopy (XPS)</i>	48
3.3	<i>FABRICATION OF Ni ALLOY AND COMPOSITES</i>	49
3.3.1	<i>Characterization of Base Alloy and Composites</i>	50
3.3.2	<i>Hardness and Density Measurement</i>	51
3.4	<i>DRY FRICTION AND WEAR TEST</i>	51
3.4.1	<i>Characterization of Worn Surfaces</i>	53
Chapter 4: <i>SYNTHESIS AND TRIBOLOGICAL BEHAVIOUR OF Ni ALLOY-BASED COMPOSITES CONTAINING Ag, Ag-rGO, AND Ag-(rGO-Ni)</i>		54
4.1	<i>RESULTS</i>	54
4.1.1	<i>Characterization of Materials</i>	54
4.1.1.1	<i>FTIR Spectra of GO, rGO, and rGO-Ni</i>	54
4.1.1.2	<i>XRD analysis of rGO and rGO-Ni</i>	55
4.1.1.3	<i>RAMAN analysis of rGO and rGO-Ni</i>	56

4.1.1.4	<i>TEM analysis of rGO and rGO-Ni</i>	57
4.1.1.5	<i>XPS analysis of rGO and rGO-Ni</i>	58
4.1.1.6	<i>Morphology of ball-milled powders and composites</i>	61
4.1.1.7	<i>Hardness and density measurements</i>	65
4.1.2	<i>Dry Sliding Friction and Wear</i>	67
4.1.2.1	<i>Variation of coefficient of friction with time</i>	67
4.1.2.2	<i>Variation of average coefficient of friction with temperature</i>	68
4.1.2.3	<i>Variation of wear rate with temperature</i>	69
4.1.3	<i>Analysis of Worn Surfaces</i>	70
4.1.3.1	<i>Electron microscopy of worn surfaces of tribo-pair</i>	70
4.1.3.2	<i>X-ray diffraction analysis of worn surface of composites</i>	83
4.1.3.3	<i>Raman analysis of the worn surface of the composites</i>	83
4.1.3.4	<i>Examination of Subsurfaces</i>	84
4.2	<i>DISCUSSION</i>	85
 Chapter 5: EFFECT OF rGO-Ni CONTENT ON TRIBOLOGICAL BEHAVIOUR OF Ni ALLOY-BASED COMPOSITES		94
5.1	<i>RESULTS</i>	94
5.1.1	<i>Characterization of Composites</i>	94
5.1.1.1	<i>Morphology of ball-milled powders and composites</i>	94
5.1.1.2	<i>Microstructure of composites</i>	96
5.1.1.3	<i>Hardness and density measurement of composites</i>	98
5.1.2	<i>Dry Sliding Friction and Wear Behaviour</i>	100
5.1.2.1	<i>Variation of coefficient of friction with time</i>	100
5.1.2.2	<i>Variation of average coefficient of friction with temperature</i>	102
5.1.2.3	<i>Variation of wear rate with temperature</i>	103

5.1.3	<i>Analysis of Worn Surfaces</i>	104
5.1.3.1	<i>Electron microscopy of worn surfaces of tribo-pairs</i>	104
5.1.3.2	<i>X-ray diffraction analysis of the worn surface of composites</i>	113
5.1.3.3	<i>Examination of Subsurface</i>	113
5.2	<i>DISCUSSION</i>	114
Chapter 6:	<i>TRIBOLOGICAL BEHAVIOUR OF Ni ALLOY-BASED COMPOSITES CONTAINING FIXED AMOUNT OF Ag, AND DIFFERENT AMOUNTS OF h-BN-Ni</i>	120
6.1	<i>RESULTS</i>	120
6.1.1	<i>Characterization of Materials</i>	120
6.1.1.1	<i>FTIR Spectra of h-BN, h-BN-O, and h-BN-O-Ni</i>	120
6.1.1.2	<i>XRD analysis of h-BN, h-BN-O, and h-BN-O-Ni</i>	121
6.1.1.3	<i>TEM analysis of h-BN-O-Ni</i>	122
6.1.1.4	<i>XPS analysis of h-BN-O and h-BN-O-Ni</i>	124
6.1.1.5	<i>Morphology of ball-milled powders and composites</i>	127
6.1.1.6	<i>X-ray diffraction analysis of ball-milled powders and composites</i>	127
6.1.1.7	<i>Microstructural analysis</i>	129
6.1.1.8	<i>Hardness and density measurement</i>	131
6.1.2	<i>Dry Sliding Friction and Wear Behaviour</i>	132
6.1.2.1	<i>Variation of coefficient of friction with time</i>	132
6.1.2.2	<i>Variation of average coefficient of friction with temperature</i>	132
6.1.2.3	<i>Variation of wear rate with temperature</i>	133
6.1.3	<i>Analysis of Worn Surfaces</i>	135
6.1.3.1	<i>Electron microscopy of worn surfaces of tribo-pairs</i>	135
6.1.3.2	<i>X-ray diffraction analysis of worn surface of composites</i>	147
6.1.3.3	<i>Raman analysis of worn surface of composites</i>	148

6.1.3.4	<i>Examination of Subsurface</i>	150
6.2	<i>DISCUSSION</i>	151
Chapter 7: TRIBOLOGICAL PERFORMANCE OF Ni ALLOY-BASED COMPOSITES CONTAINING FIXED AMOUNTS OF Ag, rGO-Ni, AND DIFFERENT AMOUNTS OF h-BN-Ni		160
7.1	<i>RESULTS</i>	160
7.1.1	<i>Characterization of Composites</i>	160
7.1.1.1	<i>Morphology of ball-milled powders and composites</i>	160
7.1.1.2	<i>Microstructure of composites</i>	162
7.1.1.3	<i>Hardness and density measurement of composites</i>	164
7.1.2	<i>Dry Sliding Friction and Wear Behaviour</i>	164
7.1.2.1	<i>Variation of coefficient of friction with time</i>	164
7.1.2.2	<i>Variation of average coefficient of friction with temperature</i>	165
7.1.2.3	<i>Variation of wear rate with temperature</i>	167
7.1.3	<i>Morphology of Worn Surfaces</i>	168
7.1.3.1	<i>Electron microscopy of worn surfaces of tribo-pairs</i>	168
7.1.3.2	<i>X-ray diffraction analysis of the worn surface of composites</i>	176
7.1.3.3	<i>Raman spectroscopy of the worn surface of composites</i>	177
7.1.3.4	<i>Examination of Subsurface</i>	178
7.2	<i>DISCUSSION</i>	179
Chapter 8: CONCLUSIONS		186
8.1	<i>Ni ALLOY-BASED COMPOSITES CONTAINING Ag, Ag-rGO, AND Ag-(rGO-Ni)</i>	186
8.2	<i>COMPOSITES CONTAINING FIXED AMOUNT OF Ag AND DIFFERENT AMOUNTS OF rGO-Ni</i>	188

8.3	<i>COMPOSITES CONTAINING FIXED AMOUNT OF Ag AND DIFFERENT AMOUNTS OF h-BN-Ni</i>	189
8.4	<i>COMPOSITES CONTAINING FIXED AMOUNTS OF Ag, rGO-Ni, AND DIFFERENT AMOUNTS OF h-BN-Ni</i>	190
	<i>FUTURE SCOPE</i>	192
	<i>REFERENCES</i>	193
	<i>LIST OF PUBLICATIONS</i>	205

List of Figures

Fig. 2. 1	Classification of Composites	8
Fig. 2. 2	Classification of the processing routes to develop MMCs	10
Fig. 2. 3	Steps involved in the powder metallurgy process	11
Fig. 2. 4	A schematic diagram of sintering	13
Fig. 2. 5	A schematic diagram of the Spark Plasma Sintering (SPS) machine	17
Fig. 2. 6	Ranges of application of various lubricants in (a) vacuum environments and (b) cryogenic and high temperature environments, and (c) radiation environments [29]	23
Fig. 2. 7	Schematic of step-by-step methodology of the present investigation	40
Fig. 3. 1	Synthesis of GO, rGO, and Ni-doped rGO via wet chemistry routes	45
Fig. 3. 2	A schematic demonstration of stepwise preparation of <i>h</i> -BN-O and <i>h</i> -BN-O-Ni	47
Fig. 4. 1	FTIR spectra of GO, rGO, and rGO-Ni, along with the assignment of vibrational peaks	55
Fig. 4. 2	XRD patterns of (a) rGO and (b) rGO-Ni, along with the assignment of diffraction features	56
Fig. 4. 3	Raman spectra of (a) rGO and (b) rGO-Ni, along with assignment of Raman active modes	57
Fig. 4. 4	TEM images of (a-c) rGO and (d-i) rGO-Ni at different magnifications. In high-resolution images (g-h) graphitic lamellae, and (e-f, h-i) Ni-based nanoparticles are explicitly seen in rGO-Ni. (j) Electron micrograph along with corresponding are a elemental mapping (C, O, and Ni) of rGO-Ni	59
Fig. 4. 5	High-resolution (a) C 1s, (b) O 1s, and (c) Ni 2p XP spectra along with deconvoluted peak components of rGO. (d) C 1s, (e) O 1s, and (f) Ni 2p XP spectra along with deconvoluted peak components of rGO-Ni	60

- Fig. 4. 6** SEM image of elemental powders (a) Ni, (b) Cr, (c) Mo, (d) Ti, (e) Al, and (f) Ag, along with (g) their XRD pattern 61
- Fig. 4. 7** FESEM images of milled powders (a) N0, (b) NA, (c) NAG, and (d) NANG 62
- Fig. 4. 8** X-ray diffraction patterns of (a) ball milled powder and (b) spark plasma sintered composite for N0, NA, NAG, and NANG 63
- Fig. 4. 9** FESEM micrographs of (a) N0, (b) NA, (c) NAG, and (d) NANG along with their corresponding area elemental distribution (Ni, Cr, Mo, Ti, Al, Ag, C) and wt.% of each element 64
- Fig. 4. 10** EDS analysis of regions (a) 1, (b) 2, and (c) 3 marked in FESEM micrograph of NANG illustrated as Fig 4.9 (d) 66
- Fig. 4. 11** Variation of coefficient of friction with time at (a) RT, (b) 200, (c) 400, (d) 600, and (e) 800 °C for N0, NA, NAG, and NANG 68
- Fig. 4. 12** Variation of average coefficient of friction for base alloy and composites with temperature 69
- Fig. 4. 13** Variation of specific wear rate for base alloy and composites with temperature 70
- Fig. 4. 14** FESEM micrographs of the worn-out base alloy (N0) and EDS of the marked region at (a and b) RT, (c and d) 200, (e and f) 400, (g and h) 600, and (i and j) 800 °C 72
- Fig. 4. 15** FESEM micrographs of the worn-out silicon nitride ball (counterface) slid against N0 along with EDS at the marked region at (a and b) RT, (c and d) 200, (e and f) 400, (g and h) 600, and (i and j) 800 °C 73
- Fig. 4. 16** FESEM micrographs of the worn-out NA and EDS of the marked region at (a and b) RT, (c and d) 200, (e and f) 400, (g and h) 600, and (i and j) 800 °C 75
- Fig. 4. 17** FESEM micrographs of the worn-out silicon nitride ball (counterface) slid against NA along with EDS at the marked region at (a and b) RT, (c and d) 200, (e and f) 400, (g and h) 600, and (i and j) 800 °C 76
- Fig. 4. 18** FESEM micrographs of the worn-out NAG and EDS of the marked region at (a

and b) RT, (c and d) 200, (e and f) 400, (g and h) 600, and (i and j) 800 °C

78

Fig. 4. 19 FESEM micrographs of the worn-out silicon nitride ball (counterface) slid against NAG along with EDS at the marked region at (a and b) RT, (c and d) 200, (e and f) 400, (g and h) 600, and (I and j) 800 °C

79

Fig. 4. 20 FESEM micrographs of the worn-out NANG and EDS of the marked region at (a and b) RT, (c and d) 200, (e and f) 400, (g and h) 600, and (i and j) 800 °C

81

Fig. 4. 21 FESEM micrographs of the worn-out silicon nitride ball (counterface) slid against NANG along with EDS at the marked region at (a and b) RT, (c and d) 200, (e and f) 400, (g and h) 600, and (i and j)

82

Fig. 4. 22 X -ray diffraction patterns of worn composite (a) N0 (b) NA, (c) NAG, and (d) NANG at different all the temperatures

84

Fig. 4. 23 Raman spectra of worn surface of (a) N0, (b) NA, (c) NAG, and (d) NANG at different temperatures

85

Fig. 4. 24 Cross-sectional FESEM micrographs of the worn subsurface at 800 °C corresponding to (a) N0, (b) NA, (c) NAG, and (d) NANG

86

Fig. 5. 1 FESEM images of milled powders (a) NANG0.5, (b) NANG1.0, (c) NANG1.5, and (d) NANG2.0

95

Fig. 5. 2 X-ray diffraction patterns of (a) ball milled powder and (b) spark plasma sintered composite for NA, NANG0.5, NANG1.0, NANG1.5, and NANG2.0

96

Fig. 5. 3 SEM micrographs of microstructure of (a) NANG0.5, (b) NANG1.0, (c) NANG1.5, and (d) NANG2.0

97

Fig. 5. 4 Area elemental mapping along with wt.% for (a) NANG0.5, (b) NANG1.0, (c) NANG1.5, and (d) NANG2.0

99

Fig. 5. 5 Variation of coefficient of friction with time at (a) RT, (b) 200, (c) 400, (d) 600, and (e) 800 °C for N0, NA, NANG0.5, NANG1.0, NANG1.5, and NANG2.0

101

Fig. 5. 6	Variation of average coefficient of friction with temperature for the base alloy and composites	102
Fig. 5. 7	Variation of specific wear rate with temperature for the base alloy and composites	103
Fig. 5. 8	FESEM micrographs of the worn-out NANG0.5 and EDS of the marked region at (a and b) RT, (c and d) 200, (e and f) 400, (g and h) 600, and (i and j) 800 °C	105
Fig. 5. 9	FESEM micrographs of the worn-out silicon nitride ball (counterface) slid against NANG0.5 along with EDS at the marked region at (a and b) RT, (c and d) 200, (e and f) 400, (g and h) 600, and (i and j) 800 °C	106
Fig. 5. 10	FESEM micrographs of the worn-out NANG1.5 and EDS of the marked region at (a and b) RT, (c and d) 200, (e and f) 400, (g and h) 600, and (i and j) 800 °C	108
Fig. 5. 11	FESEM micrographs of the worn-out silicon nitride ball (counterface) slid against NANG1.5 along with EDS at the marked region at (a and b) RT, (c and d) 200, (e and f) 400, (g and h) 600, and (i and j) 800 °C	109
Fig. 5. 12	FESEM micrographs of the worn-out NANG2.0 and EDS of the marked region at (a and b) RT, (c and d) 200, (e and f) 400, (g and h) 600, and (i and j) 800 °C	111
Fig. 5. 13	FESEM micrographs of the worn-out silicon nitride ball (counterface) slid against NANG2.0 along with EDS at the marked region at (a and b) RT, (c and d) 200, (e and f) 400, (g and h) 600, and (i and j) 800 °C	112
Fig. 5. 14	X-ray diffraction patterns of worn composite (a) NANG0.5, (b) NANG1.5, and (c) NANG2.0 at various temperatures	114
Fig. 5. 15	FESEM micrographs of cross-section of subsurface of worn track at 800 °C corresponding to (a) NANG0.5, (b) NANG1.5, and (c) NANG2.0	115
Fig. 5. 16	Features on the worn surface affecting the friction and wear behaviour under dry sliding	116

Fig. 6. 1	FTIR spectra of <i>h</i> -BN, <i>h</i> -BN-O, and <i>h</i> -BN-O-Ni along with the assignment of vibrational peaks	121
Fig. 6. 2	XRD patterns (a) <i>h</i> -BN, (b) <i>h</i> -BN-O, and (c) <i>h</i> -BN-O-Ni, along with the assignment of diffraction features	122
Fig. 6. 3	TEM images of <i>h</i> -BN-O-Ni at (a) low and (b) high magnifications. The nickel-based nanoparticles (indicated by black arrows) in a range of 2-4 nm are distributed on <i>h</i> -BN-O nanosheets. The SAED pattern with crystalline fringes of <i>h</i> -BN-O-Ni is shown as an inset of (b). (c) Micrograph of <i>h</i> -BN-O-Ni along with corresponding area elemental (B, N, O, and Ni) distribution based on EDS measurements.	123
Fig. 6. 4	Survey spectra of (a) <i>h</i> -BN-O and (b) <i>h</i> -BN-O-Ni along with assignment of spectral features	125
Fig. 6. 5	High-resolution (a) B 1s, (b) C 1s, (c) N 1s (d) O 1s, and (e) Ni 2p XP spectra along with deconvoluted peak components of <i>h</i> -BN-O. (f) B 1s, (g) C 1s, (h) N 1s, (i) O 1s, and (j) Ni 2p XP spectra along with deconvoluted peak components of <i>h</i> -BN-O-Ni	126
Fig. 6. 6	FESEM images of milled powders (a) NAh ₂ , (b) NAh ₄ , (c) NAh ₆ , and (d) NAh ₈	127
Fig. 6. 7	X-ray diffraction patterns of (a) ball milled powder and (b) spark plasma sintered base alloy and composites	128
Fig. 6. 8	FESEM micrographs for the microstructure of (a) NAh ₂ , (b) NAh ₄ , (c) NAh ₆ , and (d) NAh ₈ along with corresponding area elemental distribution	129
Fig. 6. 9	EDS of (a) region 1 and (b) region 2 marked in the microstructure of NAh ₈ in Fig. 6.8 (d)	131
Fig. 6. 10	Variation of coefficient of friction with time for (a) NAh ₂ , (b) NAh ₄ , (c)NAh ₆ , and (d) NAh ₈ at all the temperatures	133
Fig. 6. 11	Variation of average coefficient of friction for base alloy and composites with temperature	134
Fig. 6. 12	Variation of specific wear rate for the base alloy and composites with temperature	135
Fig. 6. 13	FESEM micrographs of the worn-out NAh ₂ composite and EDS of the marked region at (a and b) RT, (c and d) 200, (e and f) 400, (g and h) 600, and (i and j) 800 °C	137

- Fig. 6. 14** FESEM micrographs of the worn-out silicon nitride ball (counterface) slid against NAh2 along with EDS at the marked region at (a and b) RT, (c and d) 400, and (e and f) 800 °C 138
- Fig. 6. 15** FESEM micrographs of the worn-out NAh4 composite and EDS of the marked region at (a and b) RT, (c and d) 200, (e and f) 400, (g and h) 600, and (i and j) 800 °C 140
- Fig. 6. 16** FESEM micrographs of the worn-out silicon nitride ball (counterface) slid against NAh4 along with EDS at the marked region at (a and b) RT, (c and d) 400, and (e and f) 800 °C 141
- Fig. 6. 17** FESEM micrographs of the worn-out NAh6 composite and EDS of the marked region at (a and b) RT, (c and d) 200, (e and f) 400, (g and h) 600, and (i and j) 800 °C 143
- Fig. 6. 18** FESEM micrographs of the worn-out silicon nitride ball (counterface) slid against Nah6 along with EDS at the marked region at (a and b) RT, (c and d) 400, and (e and f) 800 °C 144
- Fig. 6. 19** FESEM micrographs of the worn-out NAh8 composite and EDS of the marked region at (a and b) RT, (c and d) 200, (e and f) 400, (g and h) 600, and (i and j) 800 °C 146
- Fig. 6. 20** FESEM micrographs of the worn-out silicon nitride ball (counterface) slid against Nah8 along with EDS at the marked region at (a and b) RT, (c and d) 400, and (e and f) 800 °C 147
- Fig. 6. 21** X-ray diffraction patterns of worn base alloy and composites at (a) RT, (b) 200, (c) 400, (d) 600, and (e) 800 °C 149
- Fig. 6. 22** Raman spectra of worn base alloy and composites at (a) RT, (b) 200, (c) 400, (d) 600, and (e) 800 °C 150
- Fig. 6. 23** Cross-sectional FESEM micrographs of the worn subsurface at 800 °C corresponding to (a) NAh2, (b) NAh4, (c) NAh6, and (d) NAh8 151
- Fig. 7. 1** FESEM micrographs of milled powders (a) NANGh2, (b) NANGh4, (c) NANGh6, and (d) NANGh8 161
- Fig. 7. 2** X-ray diffraction patterns of (a) ball milled powder and (b) spark plasma sintered composite for NANGh2, NANGh4, NANGh6, and NANGh8 162
- Fig. 7. 3** Scanning Electron micrographs of (a) NANGh2, (b) NANGh4, (c) NANGh6,

	and (d) NANGh8 along with their corresponding area elemental distribution (Ni, Cr, Mo, Ti, Al, Ag, B, N, C) and wt.% of each element	162
Fig. 7. 4	Variation of coefficient of friction with time at (a) RT, (b) 200, (c) 400, (d) 600, and (e) 800 °C for base alloy and composites	166
Fig. 7. 5	Variation of average coefficient of friction with temperature for the base alloy and composites	167
Fig. 7. 6	Variation of specific wear rate with temperature for the base alloy and composites	168
Fig. 7. 7	FESEM micrographs of the worn-out NANGh2 and EDS of the marked region at (a and b) RT, (c and d) 200, (e and f) 400, (g and h) 600, and (i and j) 800 °C	169
Fig. 7. 8	FESEM micrographs of the worn-out silicon nitride ball (counterface) slid against NANGh2 at (a) RT, (b) 400, and (c) 800 °C	170
Fig. 7. 9	FESEM micrographs of the worn-out NANGh4 and EDS of the marked region at (a and b) RT, (c and d) 200, (e and f) 400, (g and h) 600, and (i and j) 800 °C	171
Fig. 7. 10	FESEM micrographs of the worn-out silicon nitride ball (counterface) slid against NANGh4 at (a) RT, (b) 400, and (c) 800 °C	172
Fig. 7. 11	FESEM micrographs of the worn-out NANGh6 and EDS of the marked region at (a and b) RT, (c and d) 200, (e and f) 400, (g and h) 600, and (i and j) 800 °C	173
Fig. 7. 12	FESEM micrographs of the worn-out silicon nitride ball (counterface) slid against NANGh6 at (a) RT, (b) 400, and (c) 800 °C	174
Fig. 7. 13	FESEM micrographs of the worn-out NANGh8 and EDS of the marked region at (a and b) RT, (c and d) 200, (e and f) 400, (g and h) 600, and (i and j) 800 °C	175
Fig. 7. 14	FESEM micrographs of the worn-out silicon nitride ball (counterface) slid against NANGh8 at (a) RT, (b) 400, and (c) 800 °C	176
Fig. 7. 15	X-ray diffraction patterns of worn composite (a) NANGh2, (b) NANGh4, (c) NANGh6, and (d) NANGh8 at different temperatures	177

Fig. 7. 16 Raman spectra of worn surface of (a) NANGh2, (b) NANGh4, (c) NANGh6, and (d) NANGh8 at different temperatures 178

Fig. 7. 17 FESEM micrographs of cross-section of subsurface of worn track at 800 °C corresponding to (a) NANGh2, (b) NANGh4, (c) NANGh6, and (d) NANGh8 179

Fig. 7. 18 Schematic illustration for the wear mechanism of Ni alloy-based nanocomposites at (a) RT, (b) 400, and (c) 800 °C 184

List of Tables

Table 2.1	Review of the tribological properties of Ni-based high temperature self-lubricating composites	31
Table 3.1	Powders, their size, purity, and supplier	41
Table 3.2	Designation, composition, and spark plasma sintering parameters of Ni alloy-based composites	49
Table 4.1	Specimen designation, composition, density, and microhardness	65
Table 5.1	EDS analysis of marked regions in Fig. 5.3 (a)	97
Table 5.2	Specimen designation, composition, density, and microhardness	97
Table 6.1	Specimen designation, composition, density, and microhardness	131
Table 7.1	Specimen designation, composition, density, and microhardness	163

List of abbreviations & symbols

2D	:	Two dimensional
CMCs	:	Ceramic Matrix Composites
CoF	:	Coefficient of friction
EDS	:	Energy Dispersive X-ray Spectroscopy
FESEM	:	Field Emission Scanning Electron Microscopy
FTIR	:	Fourier-Transform Infrared Spectrometer
g	:	Gram
<i>h</i> -BN	:	Hexagonal Boron Nitride
hr	:	Hour
HV	:	Vickers Hardness
kHz	:	Frequency
min	:	Minute
mm ³ /Nm	:	Wear Rate
MMCs	:	Metal Matrix Composites
mL/min	:	Flow Rate
mL	:	Millilitres
MPa	:	Mega Pascal
m/s	:	Sliding Speed
mg/mL	:	Milligram per millilitre
N	:	Normal Load
Ni- <i>h</i> -BN	:	Ni-Doped Hexagonal Boron Nitride
Ni-rGO	:	Ni-Doped Reduced Graphene Oxide
P/M	:	Powder Metallurgy
PMCs	:	Polymer Matrix Composites
rpm	:	Revolution Per minute
rGO	:	Reduced Graphene oxide
RT	:	Room Temperature
S	:	Sliding Distance
SAED	:	Selected Area Electron Diffraction
SEM	:	Scanning Electron Microscopy
SPS	:	Spark Plasma Sintering

TEM	:	Transmission Electron Microscope
wt. %	:	Weight Percentage
XPS	:	X- Ray Photoelectron Spectroscopy
XRD	:	X- Ray Diffraction
°C	:	Degree Celsius
°C/min	:	Heating Rate
%	:	Percentage
μm	:	Micrometre
λ	:	Wavelength of the X-Ray
θ	:	Incident Angle
γ	:	Gamma